COMPUTER VISION AND IMAGE UNDERSTANDING
Vol. 61, No. 1, January, pp. 122–137, 1995

Optimal Sensor and Light Source Positioning for Machine Vision[1]

SEUNGKU YI,[2] ROBERT M. HARALICK, AND LINDA G. SHAPIRO

Intelligent Systems Laboratory, FT-10, University of Washington, Seattle, Washington 98195

Received August 15, 1993; accepted April 22, 1994

An optimization approach to automatic sensor and light source positioning for a machine vision task, where geometric measurement and/or object verification is important, is discussed. The goal of the vision task is assumed to be specified in terms of measurements related to edges. The optimal sensor and light source positions are defined in such a way that when the sensor and light source are placed in the optimal positions, we can obtain a picture which produces the minimum variance for the required measurement. Experiments show that the uncertainty in the edge point position is inversely proportional to the contrast across the edge. Using a variant of the Torrance-Sparrow model that takes into account the polarization of the light, the contrasts across edges are computed and used to estimate the variance of the required 2D measurement. An optimization procedure employing mathematical programming techniques uses this information to determine the best positions for the light source and sensor in order to perform the required measurement. A series of experiments was conducted to demonstrate the feasibility of our optimization approach. The optimal positions computed by the program were found to be the best ones in the real experiments. Furthermore, the correlation coefficient between the expected variance and the variance computed from the real pictures was 0.768.

1. INTRODUCTION

A typical computer vision system can be decomposed functionally into three subsystems: the image acquisition subsystem, the image processing subsystem, and the image understanding subsystem. The image acquisition subsystem is responsible for providing pictures to the image processing subsystem, which analyzes pictures and generates low-level information, such as edges and regions, in order for the image understanding subsystem to produce an inference relative to a scene description or object mensuration.

A vision system's performance depends on the image quality which is affected directly by illumination. To obtain the best result, the object must be illuminated in such a way that distinctions between object surfaces are as clear as possible. Although researchers set up the image acquisition environment as best they can, until recently lighting devices have been regarded as passive components in machine vision research. There have been very few efforts to select or to optimally position lighting devices [2, 4, 20]. If illumination is controlled in an active way, better quality images can be obtained without further investment. It is less costly to produce high-quality images by controlling the light source than to develop complex image processing algorithms for low-quality images.

There has been some work done on sensor and illumination planning. Pentland studied how a mobile robot can obtain depth information using depth of field [21]. Krotokov studied the relationship between lens focusing and depth of field [21]. Krotokov studied the relationship between lens focusing and depth of field [16]. Both of these were related to lens selection. Ikeuchi concentrated on view class classification rather than on camera and illumination control [12, 13]. Shirai and Tsuji were two of the first researchers who took advantage of controlled illumination in extracting line drawings from images of 3D objects [23]. Their idea was to remove shadow effects by controlling illumination directions. Cowan and Kovesi studied automatic determination of sensor location [4], and their approach is to formulate a constraint satisfaction problem. VIO (vision illumination object) developed by Niepold and Sakane may be the first system that considered camera, illumination, and features simultaneously [19]. Yi *et al.* proposed a heuristic optimality criteria in terms of edge visibility for the optimal sensor and light source position and demonstrated that the optimization approach is feasible and can be solved by mathematical programming techniques [27].

In this paper, we will describe an illumination control system called ICE (illumination control expert) that determines the optimal sensor and light source position for a given vision task. A vision task is specified by an object model that includes photometric properties, as well as geometric properties of the target object and the required measurements. We consider only 2D measurements that can be determined after the positions of certain feature

[1] This research was supported partly by the National Science Foundation, Grant DMC-871480 9.

[2] Seungku Yi is now with Software Research Laboratory at Daewoo Telecom Ltd., Seoul, Korea.

1077-3142/95 $6.00

points are detected. The distance between two corner points and the angle made by two lines are typical examples. To compute the distance between two points, the two endpoints must be determined. To compute the angle made by two lines, three points must be determined. A point may be the intersection of two lines, the center of a circle, or the center of an ellipse. Lines, circles, and ellipses are determined from edge points in 2D images. Uncertainties in the positions of edge points are propagated all the way to the measurement. Our approach to solve this illumination problem is to formulate an optimization problem in terms of variance of the requirement measurement and take advantage of mathematical programming techniques.

ICE automatically finds the optimal sensor and light source positions, producing an image from which the measurement data can be obtained with the minimum uncertainty. The following must be known: geometry of the object, photometric properties of the object, object edges involved in the given task, measurement type, and light source type. The light source is assumed to be a point light source, and no area light sources are supported. The background must be dark enough to distinguish the object clearly from the background. No secondary reflection or ambient light is considered. The reflectance coefficient must be known in advance, and it should be uniform over a given surface of the given object. The object edges must be able to be represented by the PADL object description language [11], and no arbitrary curves are supported.

ICE would be useful in an inspection task, where a geometric model of the object is available, and the task is to inspect manufactured instances of the object to ensure that they are not misshapen or flawed. This paper describes the ICE system and the theory behind it. We begin by defining the illumination model that is used to predict the intensity values of image points. The intensity of an image point is dependent on the reflectivity of the corresponding point on the object, the optical devices, and the lighting.

2. ILLUMINATION MODEL

We assume that all surfaces of an object have the same photometric properties, and thus they have the same bidirectional reflectance function (BDRF). We also assume that the incident light is polarized and employ the illumination model developed by Yi *et al.* [9, 26].

Let $\vec{N}$ be the unit normal vector to a given surface at a certain surface point, and let $\vec{L}$ be the unit vector in the direction of the light source from the given surface point. From [26], we know that

$$I = \int CSQ(\lambda)\, d\omega \vec{N} \cdot \vec{L}(R_{\parallel}(\lambda)J^{i}_{\parallel}(\lambda) + R_{\perp}(\lambda)J^{i}_{\perp}(\lambda))\, d\lambda, \tag{1}$$

where C is the lens collection, S is the sensor responsivity, Q is the spectral distribution function of the illumination source, $R_{\parallel}$ is the bidirectional function for the incident light that is parallelly polarized, and $R_{\perp}$ is the bidirectional function for the incident light that is perpendicularly polarized. From [26], we also know that

$$R_{\parallel} = sK\rho_{\parallel} + (1 - s)R_{d},$$
$$R_{\perp} = sK\rho_{\parallel} + (1 - s)R_{d},$$

where

$$K = \frac{DG}{\pi(\vec{N} \cdot \vec{L})(\vec{N} \cdot \vec{V})}.$$

$R_{\parallel}$ and $R_{\perp}$ are reflectance coefficients for the specular reflection, and R_d is the reflectance coefficient for diffusion. D is a surface roughness distribution function, and G is the geometric attenuation factor. The surface roughness D is assumed to have a Beckmann distribution and is given by

$$D = \frac{1}{m^2 \cos^4 \beta} \exp\left(-\left(\frac{\tan \beta}{m}\right)^2\right),$$

where m is a constant and β is a variable. If $\vec{H}$ is the unit vector that bisects the angle between $\vec{L}$ and $\vec{V}$, then

$$\vec{H} = \frac{\vec{L} + \vec{V}}{\|\vec{L} + \vec{V}\|}.$$

Thus G can be written as

$$G = \min\left\{1, \frac{2(\vec{N} \cdot \vec{H})(\vec{N} \cdot \vec{V})}{\vec{V} \cdot \vec{H}}, \frac{2(\vec{N} \cdot \vec{H})(\vec{N} \cdot \vec{L})}{\vec{L} \cdot \vec{H}}\right\}.$$

From [26], we also know that

$$\rho_{\perp}(\psi) = \frac{a^2 + b^2 - 2a \cos \psi + \cos^2 \psi}{a^2 + b^2 + 2a \cos \psi + \cos^2 \psi},$$

$$\rho_{\parallel}(\psi) = \rho_{\perp}(\psi) \frac{a^2 + b^2 - 2a \sin \psi \tan \psi + \sin^2 \psi \cos^2 \psi}{a^2 + b^2 + 2a \sin \psi \tan \psi + \sin^2 \psi \tan^2 \psi},$$

where ψ is the incidence angle, and a and b are quantities related to the incidence angle ψ, the refractive index n, and the extinction coefficient k of the material. They are

$$a = \sqrt{\frac{\sqrt{c^2 + 4n^2k^2} + c}{2}},$$

$$b = \sqrt{\frac{\sqrt{c^2 + 4n^2k^2} - c}{2}},$$

where

$$c = n^2 - k^2 - \sin^2 \psi.$$

In fact, $\rho_{\|}$ and $\rho_{\perp}$ are dependent on the wave length λ of the incident light because the refractive index and extinction coefficients are dependent on the wave length, and the Fresnel equations are good for the monochromatic wave.

3. ERROR PROPAGATION IN VISION TASKS

Suppose the distance between two corner points in a 2D image is to be measured. To measure the distance, the positions of the points must be determined. Since the true positions are usually not known, they must be estimated from the given data. Because a corner point is an intersection of two nonparallel lines, to determine the position of the corner point, the lines that pass through the corner point must be detected. A line can be determined by fitting edge points which are supposed to be on that line. There are many ways to fit a line to points. Least-squares line fitting is widely used for this purpose. To find the line, its edge points must be detected. Since images have numerous sources of error, the edge points produced by a typical edge operator are not necessarily true edges. This means that there are uncertainties in the edge point positions. Since lines are estimated by fitting noisy edges, the parameters of the fitted lines also have uncertainties coming from the uncertainties of the edge point positions. A corner point can be determined by finding the intersection point of the two fitted lines. Therefore, the position of the corner point has uncertainty that comes from the uncertainties of the fitted line parameters. Finally, since the distance between the two corner points is computed using their positions, the measured distance has uncertainties of the two corner point positions.

Haralick analyzed how edge point position uncertainty is propagated to the fitted line parameter uncertainty [8]. In his analysis, the noise is assumed to come from an independent and identical distribution. Yi *et al.* [25, 28] generalized Haralick's derivation for the case that the noise comes from an independent, but nonidentical distribution. The validity of these derivations have been proved by experiments. Error propagation was thoroughly analyzed, and the relationship between the variances of edge point positions and the expected variance of the measurement was derived. The least-squares principle was applied for line, circle, and ellipse fitting. In this paper, we employ those results.

3.1. *Noise Model*

Let (x_i, y_i) be the true, but unknown, coordinates of the ith edge point and $(\hat{x}_i, \hat{y}_i)$ be a noisy observation of (x_i, y_i). Our model for $(\hat{x}_i, \hat{y}_i)$ is

$$\hat{x}_i = x_i + \xi_i, \quad \hat{y}_i = y_i + \eta_i,$$

where the random perturbations ξ_i and η_i are assumed to be independently distributed with mean 0 and variance σ_i^2 and to come from a distribution which is an even function. Hence,

$$E[\xi_i] = E[\eta_i] = 0,$$

$$V[\xi_i] = V[\eta_i] = \sigma_i^2$$

$$E[\xi_i \xi_j] = \begin{cases} \sigma_i^2 & \text{if } i = j \\ 0 & \text{otherwise} \end{cases},$$

$$E[\eta_i \eta_j] = \begin{cases} \sigma_i^2 & \text{if } i = j \\ 0 & \text{otherwise} \end{cases},$$

and

$$E[\eta_i \xi_j] = 0.$$

3.2. *Variances of Least-Squares Estimates of Line Parameters*

Consider a situation in which points (x_i, y_i), $i = 1, \ldots, I$, are assumed to lie on an unknown straight line, and the problem is to determine the parameters of the line. Then suppose each point (x_i, y_i) satisfies the model

$$\alpha x_i + \beta y_i + \gamma = 0 \quad i = 1, \ldots, I, \tag{2}$$

where $\alpha^2 + \beta^2 = 1$. Since our noise model is not i.i.d. and all σ_i^2 are known *a priori*, we define weighted mean and weighted variance instead of arithmetic mean or variance. Let the weight be $w_i = 1/\sigma_i^2$, and define

$$\mu_x = \frac{1}{W} \sum_{i=1}^{I} w_i x_i, \qquad \mu_y = \frac{1}{W} \sum_{i=1}^{I} w_i y_i,$$

$$\sigma_x^2 = \frac{1}{\tilde{W}} \sum_{i=1}^{I} w_i (x_i - \mu_x)^2, \quad \sigma_y^2 = \frac{1}{\tilde{W}} \sum_{i=1}^{I} w_i (y_i - \mu_y)^2,$$

$$\sigma_{xy} = \frac{1}{\tilde{W}} \sum_{i=1}^{I} w_i (x_i - \mu_x)(y_i - \mu_y),$$

where

$$W = \sum_{i=1}^{I} w_i, \quad \tilde{W} = \frac{I-1}{I} W.$$

Then, from [25], we know that the variances and covariances of the line parameters are

$$
\begin{aligned}
V(\hat{\alpha}) &= \beta^2 T, \\
V(\hat{\beta}) &= \alpha^2 T, \\
V(\hat{\gamma}) &= \left(\mu_x^2 + \mu_y^2 - \gamma^2 + \frac{1}{W}\right) T + \frac{I}{W}, \\
\mathrm{Cov}(\hat{\alpha}, \hat{\beta}) &= -\alpha\beta T, \\
\mathrm{Cov}(\hat{\alpha}, \hat{\gamma}) &= \beta(-\mu_x\beta + \mu_y\alpha)T, \\
\mathrm{Cov}(\hat{\beta}, \hat{\gamma}) &= \alpha(\mu_x\beta - \mu_y\alpha)T,
\end{aligned} \tag{3}
$$

where

$$
T = \frac{\sigma_x^2 + \sigma_y^2 + I/W}{\bar{W}(\sigma_x^2 + \sigma_y^2)^2}. \tag{4}
$$

3.3. *Variance of Corner Point Position and Distance Between Points*

As derived in [25] the variance of the intersection point (r, c) of two straight lines $\alpha_1 x + \beta_1 y + \gamma_1 = 0$ and $\alpha_2 x + \beta_2 y + \gamma_2 = 0$ is

$$
\begin{aligned}
V(\hat{r}) &= \frac{1}{(\alpha_1\beta_2 - \alpha_2\beta_1)^2}\,[\beta_2^2 E[(\hat{\alpha}_1 r + \hat{\beta}_1 c + \hat{\gamma}_1)^2] \\
&\quad + \beta_1^2 E[(\hat{\alpha}_2 r + \hat{\beta}_2 c + \hat{\gamma}_2)^2]], \\
V(\hat{c}) &= \frac{1}{(\alpha_1\beta_2 - \alpha_2\beta_1)^2}\,[\alpha_2^2 E[(\hat{\alpha}_1 r + \hat{\beta}_1 c + \hat{\gamma}_1)^2] \\
&\quad + \alpha_1^2 E[(\hat{\alpha}_2 r + \hat{\beta}_2 c + \hat{\gamma}_2)^2]], \\
\mathrm{Cov}(\hat{r}, \hat{c}) &= \frac{1}{(\alpha_1\beta_2 - \alpha_2\beta_1)^2}\,[-\alpha_2\beta_2 E[(\hat{\alpha}_1 r + \hat{\beta}_1 c + \hat{\gamma}_1)^2] \\
&\quad - \alpha_1\beta_1 E[(\hat{\alpha}_2 r + \hat{\beta}_2 c + \hat{\gamma}_2)^2]],
\end{aligned} \tag{5}
$$

where

$$
\begin{aligned}
E[(\hat{\alpha} r + \hat{\beta} c + \hat{\gamma})^2] &= r^2 V(\hat{\alpha}) + c^2 V(\hat{\beta}) + V(\hat{\gamma}) \\
&\quad + 2rc\,\mathrm{Cov}(\hat{\alpha}, \hat{\beta}) + 2r\,\mathrm{Cov}(\hat{\alpha}, \hat{\gamma}) \\
&\quad + 2c\,\mathrm{Cov}(\hat{\beta}, \hat{\gamma}).
\end{aligned}
$$

Finally the variance of the distance between two points (r_1, c_1) and (r_2, c_2) is

$$
\begin{aligned}
V(\hat{d}) &= \frac{1}{d^2}\,[(r_1 - r_2)^2[V(\hat{r}_1) + V(\hat{r}_2)] \\
&\quad + (c_1 - c_2)^2[V(\hat{c}_1) + V(\hat{c}_2)] \\
&\quad + 2(r_1 - r_2)(c_1 - c_2)[\mathrm{Cov}(\hat{r}_1, \hat{c}_1) + \mathrm{Cov}(\hat{r}_2, \hat{c}_2)]].
\end{aligned} \tag{6}
$$

4. SOURCE OF MEASUREMENT UNCERTAINTY

In the previous section, we have shown how uncertainties of edge point positions in a 2D image are propagated through the 2D measurements. In this section, we will discuss the nature of the uncertainty of measurement and how to compute it. From the previous section all the final measurements have variances related to the following entity T defined by Eq. (4),

$$
T = \frac{\sigma_x^2 + \sigma_y^2 + I/W}{\bar{W}(\sigma_x^2 + \sigma_y^2)^2},
$$

where I is the number of edge points, σ_x^2 and σ_y^2 are the variances of the x and y coordinates of the edges, W is the sum of the reciprocal of the variances of each edge point coordinate over all the edges, and $\bar{W} = (I - 1)W/I$. Thus the measurement has several sources of uncertainty: edge point position uncertainty (W and $\bar{W}$) and edge visibility ($\sigma_x^2 + \sigma_y^2$ and I).

Edge point position in a 2D image is affected by noise, and there are many different types of noise in images. Some of these are caused by the image signal, while others are independent of the signal. Some noise in one edge point is related to noise in other edge points, but others are uncorrelated. Examples of commonly encountered kinds of noise can be found in [22]. Some can be controlled, but others cannot be controlled. Gray scale noise due to the sensor and noise due to the surface reflection texture are not controllable. Since we use edge operators and contrast thresholds to detect edge points, edge point positions have uncertainties depending on the contrast across the edge and on the characteristics of the edge operator used. The effect of an edge operator will be considered constant for all edge points.

To explore the relationships among the standard deviation of the random perturbation of edge position σ, the standard deviation of the additive noise σ_ξ, and the contrast C across an edge, we conducted experiments on images to empirically determine the relationship. The facet operator [7, 10] was used to detect edges. Figure 1 shows how the standard deviation of random perturbation of edge point position σ was related to the ratio of the standard deviation of additive noise to contrast in our experiments. The definition of signal-to-noise ratio, SNR, comes from information theory

$$
\mathrm{SNR} = 20 \log_{10} \frac{C}{\sigma_\xi}.
$$

There is a linear relationship between σ and σ_ξ/C when $\sigma_\xi/C < 1$ (SNR is high). There is another linear relationship that is different from this when $\sigma_\xi/C > 1$ (SNR is low). The unit of the standard deviation is the number of pixel positions, and each point in the plot represents 100 samples. When the SNR is low, the effect of contrast to the random perturbation of edge position is negligible, because the noise domainates the signal. Therefore, we

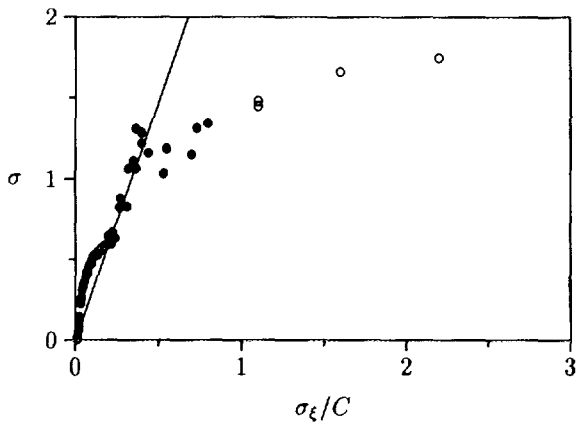

FIG. 1. Relationship between the standard deviation of the random perturbation of edge point position σ and the ratio of the standard deviation of additive noise to contrast σ_ξ/C is illustrated.

are only interested in the case where the SNR is high. The solid line in the plot is the weighted least-squares fit of all the points, except the four outliers. This least-squares fit shows the apparent linear relationship between σ and σ_ξ/C.

Now we can safely assume that the uncertainty in the edge point position is inversely proportional to the contrast across the edge and is proportional to the uncontrollable noise which is constant for all the edge points. In other words, the variance of the ith edge point position, σ_i^2, is

$$\sigma_i^2 = \frac{k\sigma_\xi^2}{C_i^2}, \tag{7}$$

where k is the constant for edge operator effect, σ_ξ^2 is the variance of an uncontrollable random additive noise (measured in units of pixels), and C_i is the contrast across the ith edge. This assumption was validated by a series of statistical tests described in [25].

5. CONTRAST EVALUATION

Since the uncertainty of the edge point position is inversely proportional to the contrast across the edge point, the computation of contrast across the edge must be discussed. Contrast is very important, since most intensity-based image processing algorithms use the contrast between regions or across regions as their criterion. Most region-growing algorithms work with average intensity, and most edge-detection algorithms work with local gradient. In this section, we will define the computation of the contrast across an edge point.

We use an object coordinate system with a reference point on the given 3D object as its origin O. Let $\vec{l} = (l_x, l_y, l_z)'$ and $\vec{v} = (v_x, v_y, v_z)'$ be position vectors of the light and sensor, respectively, seen from O. Let S be a 3D object surface. Then, S can be represented by an implicit surface function $f(x, y, z) = 0$ or by a parameterized vector form $\vec{r} = \vec{r}(\xi, \eta)$ [5]. The unit normal vector to the surface $f(x, y, z) = 0$ is given by

$$\vec{N} = \frac{\nabla f}{|\nabla f|},$$

where

$$\nabla f = \frac{\partial f}{\partial x}\vec{i} + \frac{\partial f}{\partial y}\vec{j} + \frac{\partial f}{\partial z}\vec{k},$$

or by

$$\vec{N} = \frac{(\partial\vec{r}/\partial\xi) \times (\partial\vec{r}/\partial\eta)}{\|(\partial\vec{r}/\partial\xi) \times (\partial\vec{r}/\partial\eta)\|}.$$

Let $\vec{p}$ be a point on S with coordinates (p_x, p_y, p_z). Then the unit vectors $\vec{L}$ and $\vec{V}$, denoting the light and sensor positions seen from $\vec{p}$, are given by

$$\vec{L} = \frac{\vec{l} - \vec{p}}{\|\vec{l} - \vec{p}\|} = \frac{(l_x - p_x, l_y - p_y, l_z - p_z)'}{\sqrt{(l_x - p_x)^2 + (l_y - p_y)^2 + (l_z - p_z)^2}}, \tag{8}$$

$$\vec{V} = \frac{\vec{v} - \vec{p}}{\|\vec{v} - \vec{p}\|} = \frac{(v_x - p_x, v_y - p_y, v_z - p_z)'}{\sqrt{(v_x - p_x)^2 + (v_y - p_y)^2 + (v_z - p_z)^2}}. \tag{9}$$

As in Fig. 2, let S_1 and S_2 be adjacent object surfaces. Let $\vec{r}$ be a point on the intersection curve. Let $\vec{M}_j$ be the

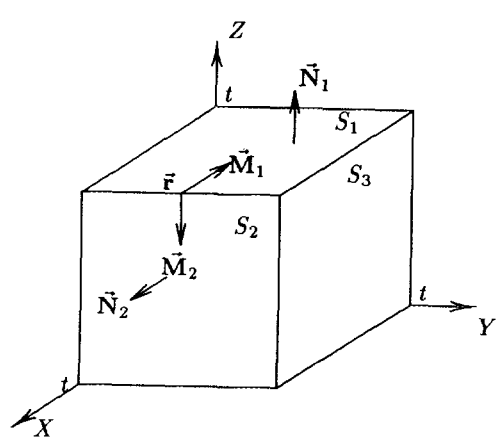

FIG. 2. A cube whose edge length is t is shown. Three of its edges are aligned along the three coordinate axes.

unit vector perpendicular to both $\vec{N}_j$ and $S_1 \cap S_2$ and on the surface S_j for $j = 1, 2$. Let $\vec{p}_j$ be a point on S_j located at a distance ζ_j away from $\vec{r}$ along $\vec{M}_j$. Explicitly,

$$\vec{p}_1 = \vec{r} + \zeta_1 \vec{M}_1, \quad \vec{p}_2 = \vec{r} + \zeta_2 \vec{M}_2.$$

Assume that ζ_1 and ζ_2 are very small, and therefore $\vec{p}_1$ and $\vec{p}_2$ are close to each other. The contrast at an edge point $\vec{r}$ is defined as the 3D contrast, the difference of the intensity of the reflected light between two small patches with centers at $\vec{p}_1$ and $\vec{p}_2$. We do consider perspective effects, since the error between 2D contrast and 3D contrast is believed to be reasonably bounded by a small value. The position vectors of the light source $\vec{L}_j$ and the sensor $\vec{V}_j$ at each $\vec{p}_j$ can be represented in terms of $\vec{l}$, $\vec{v}$, and $\vec{p}_j$ using Eqs. (8) and (9).

Assume that the effects of lens collection C and the sensor responsibility S are negligible, and the incident light is monochromatic with wavelength λ. Let J^i be the incident light and J^r be the reflected light. Let R^1 and R^2 be the bidirectional reflectance functions of two surfaces. Then the contrast between the two small patches can be computed as

$$|J_1^r - J_2^r| = |\vec{N}_1 \cdot \vec{L}_1(R_\parallel^1 J_\parallel^i + R_\perp^1 J_\perp^i) - \vec{N}_2 \cdot \vec{L}_2(R_\parallel^2 J_\parallel^i + R_\perp^2 J_\perp^i)|. \quad (10)$$

6. THE VIEWING SPACE

Since we know how to compute the contrast across an edge and what the edge visibility means, we are ready to compute the uncertainty of the measurement. To compute the measurement uncertainty, we must know the positions of sensor and light source. In ICE, the sensor is assumed to always point to an object reference point, and the sensor and the light sources are placed on the surface of a sphere with its center at the origin of the object coordinate system. We will call this sphere a reference sphere. The radius of the reference sphere is assumed to be large enough to contain the whole object. Any point on the surface of the reference sphere can be referenced by two angles, one measured from the north pole and the other from the arbitrarily chosen reference line along the equator (see Fig. 3). The viewing space is defined as the set of all points on the surface of the reference sphere.

Every point on the surface is an element of the viewing space. However, the viewing space is a contiguous space and has an infinite number of elements. How can we approximate the contiguous viewing space by a discrete space? There are many alternatives as in [13, 14, 19]. We chose to approximate the viewing space in such a way that the distance between any neighboring two points in the viewing space is approximately the same. In summary,

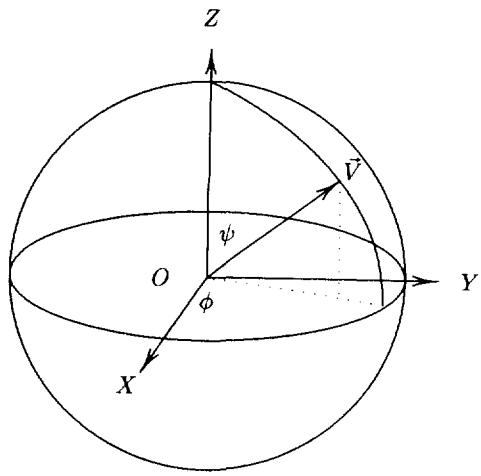

FIG. 3. A reference sphere is shown. The origin of the object coordinate system is placed at the center of the reference sphere. A point on the surface of the reference sphere is referenced by two angles: (ψ, ϕ).

- The polar angle ψ is divided every 1°.
- When $\psi = 90°$, the azimuth angle ϕ is divided into 360 intervals.
- When $\psi = 0°$ or 180°, the azimuth angle ϕ is not divided at all.
- Otherwise, the azimuth angles are divided in such a way that the solid angles each surface patch subtends are approximately equal.

As shown in Fig. 4, the solid angle a surface patch subtends is

$$d\omega = \sin \psi \, d\psi \, d\phi.$$

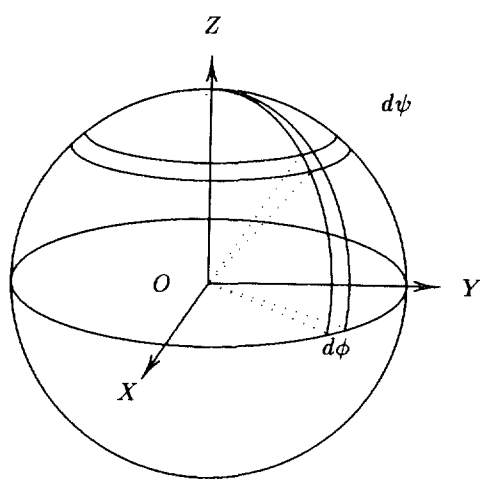

FIG. 4. The viewing space is approximated in such a way that the distance between any neighboring two points in the viewing space is approximately the same. In other words, $d\psi \, d\phi \sin \psi$ is approximately constant.

$$
\begin{array}{ccccccc}
(0,0) & & & & & & \\
(1,0) & (1,1) & \cdots & (1,6) & & & \\
(2,0) & (2,1) & \cdots & \cdots & (2,12) & & \\
\vdots & \vdots & \ddots & \ddots & \ddots & \ddots & \\
(90,0) & (90,1) & \cdots & \cdots & \cdots & \cdots & (90,359) \\
\vdots & \vdots & \ddots & \ddots & \ddots & \ddots & \\
(178,0) & (178,1) & \cdots & \cdots & (178,12) & & \\
(179,0) & (179,1) & \cdots & (179,6) & & & \\
(180,0) & & & & & &
\end{array}
$$

FIG. 5. Points in the discrete viewing space VS.

Since $d\psi$ is constant for all ψ, $d\omega$ is dependent only on $\sin\psi\, d\phi$, and we want to keep the arc length $\sin\psi\, d\phi$ constant for all possible ψ. When the polar angle of ψ is fixed, the length of the perimeter of the cross-sectional circle is $2\pi \sin\psi$. In order to keep the arc length $\sin\psi\, d\phi$ constant for all possible ψ, $360 \sin\psi$ intervals are needed to divide azimuth angle ϕ. In other words, the polar angle is divided into 1° intervals and the azimuth angle is divided into $(1/\sin\psi)°$ intervals. Thus the discrete viewing space VS is defined by

$$\mathrm{VS} = \left\{(i, j) \mid 0 \le i \le 180,\ 0 \le j \le \left\lfloor 360 \sin\left(\frac{\pi}{180} i\right)\right\rfloor\right\},$$

where i and j are integers. An element (i, j) of the discrete viewing space represents a point on the surface of the referential sphere whose spherical coordinate is

$$\frac{\pi}{180}\left(i, \frac{j}{\sin i}\right),$$

when $i \neq 0$, 180. If $i = 0$ or $i = 180$, j must be zero. The element (0, 0) of the discrete viewing space corresponds to the north pole, and the element (180, 0) corresponds to the south pole. There are

$$2\sum_{\psi=0}^{90} [360 \sin\psi] - 360 + 1 = 41{,}348$$

view points in VS; one of the enumerations of VS is shown in Fig. 5.

7. TASK SPECIFICATION

The tasks we consider are measurements of entities in a 2D image. To obtain the measurement data, features such as vertices, edges, faces, or holes, which are involved in the measurement task in the 2D image, must be detected. The required measurements can be specified in terms of these features. Since the measurements we consider can always be determined when the point positions involved are known, and those points are either vertices or the centers of holes which can be obtained using neighboring edge information, the requirements for the vision task can be stated in terms of the object edges.

Let E be the set of all edges of the given object. A required edge list, denoted by REL, is a set whose elements are subsets of E. An element of a REL is a set of object edges that we want to appear in the image at the same time. For instance, suppose we want to measure the distance between vertex v_3 and vertex v_6 of the block shown in Fig. 6. To measure the required distance, it must be possible to determine the positions of the two vertices v_3 and v_6. Since the three edges, e_2, e_4, and e_9 define the vertex v_3, at least two of the three edges must be shown in the image. Similarly, to determine the position of the vertex v_6, two of edges e_6, e_7, and e_{11} must appear in the image. The required edge list REL for this example is

$$\begin{aligned} \mathcal{A} &= \{\{e_2, e_4\}, \{e_2, e_9\}, \{e_4, e_9\}\}, \\ \mathcal{B} &= \{\{e_6, e_7\}, \{e_6, e_{11}\}, \{e_7, e_{11}\}\}, \\ \mathrm{REL} &= \{A \cup B \mid A \in \mathcal{A}, B \in \mathcal{B}\}. \end{aligned} \tag{11}$$

8. OPTIMIZATION PROCEDURE

We have shown how the uncertainty of the edge point position is propagated all the way to the measurement and have derived the expected variance of the measurements when the uncertainties of the edge point position are known. We also described the nature of the edge point position uncertainty, how to compute contrast across an edge point, the viewing space, and the vision task specification and discussed the relationship between

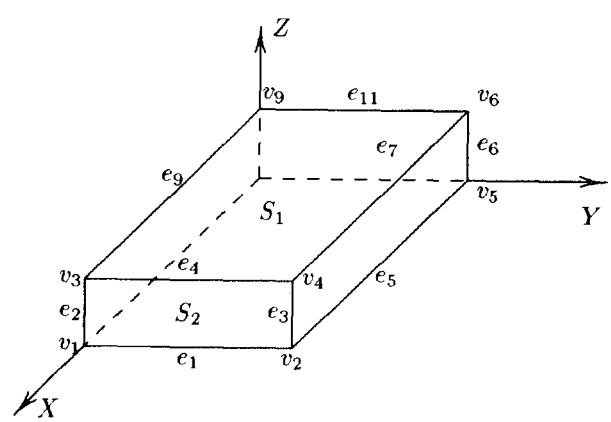

FIG. 6. A block whose sides are of length 1.25, 0.75, and 0.25 is shown. We want to measure the distance between two vertices v_3 and v_6.

procedure *Optimize*

step c1 : **for each** $\mathrm{REL}_i \in \mathrm{REL}$,

1. **call** *FindSensorLight*(REL_i),
2. **let** the optimal solution for REL_i be $(\mathbf{v}_i, \mathbf{l}_i, V_i)$.

step c2 : **return** $(\mathbf{v}_o, \mathbf{l}_o, V_o)$ where $V_o \leq V_i$ for all i.

procedure *FindSensorLight*(REL_i)

step r0 : **choose** the initial sensor position $\mathbf{v}_i^{(0)}$.

step r1 : **call** *FindLightWithFixedSensor*$(\mathbf{v}_i^{(0)}, \mathbf{l}_i^{(0)}, V^{(0,0)})$.

step r2 : **let** $j := 0$.

step r3 : **call** *FindSensorWithFixedLight*$(\mathbf{l}_i^{(j)}, \mathbf{v}_i^{(j+1)}, V^{(j+1,j)})$.

step r4 :

1. **if** $V^{(j+1,j)} > V^{(j,j)}$, **report error** and **stop**.
2. **if** $\mathbf{v}_i^{(j)} = \mathbf{v}_i^{(j+1)}$, **return** optimal solution $(\mathbf{l}_i^{(j)}, \mathbf{v}_i^{(j+1)}, V^{(j+1,j)})$.

step r5 : **call** *FindLightWithFixedSensor*$(\mathbf{v}_i^{(j+1)}, \mathbf{l}_i^{(j+1)}, V^{(j+1,j+1)})$.

step r6 :

1. **if** $V^{(j+1,j+1)} > V^{(j+1,j)}$, **report error** and **stop**.
2. **if** $\mathbf{l}_i^{(j)} = \mathbf{l}_i^{(j+1)}$, **return** optimal solution $(\mathbf{l}_i^{(j+1)}, \mathbf{v}_i^{(j+1)}, V^{(j+1,j+1)})$

step r7 : **let** $j := j + 1$ and **goto step r3**.

FIGURE 7

the edge point position uncertainty and the contrast across the edge.

Now we are ready to answer the question: *where should the sensor and light source be placed in order to obtain the best image?* There may be many different ways to define the best image; our definition of the best image is *the image from which we obtain the measurement data with the minimum variance.*

Figures 7 and 8 show a pseudocode description of our optimization procedure. The procedure *FindLightWith FixedSensor*($\mathbf{v}$, $\mathbf{l}$, V) returns the best light position $\mathbf{l}$ and the variance $\mathbf{V}$ for fixed sensor position $\mathbf{v}$. The procedure *FindSensorWithFixedLight*($\mathbf{v}$, $\mathbf{l}$, V) returns the best sensor position $\mathbf{v}$ and the variance $\mathbf{V}$ for fixed light position $\mathbf{l}$. The variance evaluation module *VarianceEvaluate*($\mathbf{v}$, $\mathbf{l}$, V) takes the sensor and light source positions, ($\mathbf{v}$, $\mathbf{l}$), as input and returns the expected variance $\mathbf{V}$ of the required measurements. Suppose a vision task specification is given and the REL is known. Then, the perspective projection of each edge in each element of REL is computed. From this computation the information about how the edge points are spatially distributed in the 2D image, i.e., μ_x, μ_y, $(\sigma_x^2 + \sigma_y^2)$, is obtained. The 3D transformations can be found in a standard computer graphics text such as [18]. The variance of the random perturbations of each edge point along a given edge, σ_i^2, and sum of its reciprocals, W, are computed using the contrast across the edge point (Eqs. (10) and (7)). Using this information, the variances of line parameters are obtained (Eq. (3)). The variance of the intersection point of two edges can now be computed using Eq. (5). Then Eq. (6) gives the variance of the measurement between two points.

For a given element of REL, finding the optimal sensor and light source position involves a highly nonlinear, four-dimensional search space, since the sensor and the light source positions are each indexed by two variables: polar angle and azimuth angle. Since we tesselated the viewing space into a finite number of positions, the search space is a discrete four-dimensional space. If the space is not convex, we cannot always find the global minimum. However, the experiments described in Section 9 assure us that the two-dimensional space, which is obtained by fixing either the sensor position or the light source position, is convex, and there is only one global maximum.

Wendell and Hurter proposed an alternating technique for a class of mathematical programs in which the vector variable is partitioned into two independent subvectors [24]. Let u and v be two such subvectors. Their approach is to solve the problem for u while keeping v constant and then solve the problem for v while keeping u as the solution found in the first step. The roles of u and v are kept

procedure *FindLightWithFixedSensor*($\mathbf{v}, \mathbf{l}, \mathbf{V}$)

step s0 : **choose** the initial light position $\mathbf{l}^{(0)}$ and **let** $k := 0$.

step s1 : **find** the neighbors of $\mathbf{l}^{(k)}$ and **let** the neighbors be $\mathrm{N} = \{\mathbf{l}_1^{(k)}, \ldots, \mathbf{l}_m^{(k)}\}$.

step s2 : **for each** $\mathbf{l} \in \{\mathbf{l}^{(k)}\} \bigcup \mathrm{N}$, **call** *VarianceEvaluate* with $\mathbf{v}$ and $\mathbf{l}$. **Let** the expected variances be called $V^{(k)}, V_1^{(k)}, \ldots, V_m^{(k)}$.

step s3 : **if** $V^{(k)} < V_j^{(k)}$ for all $j = 1, \ldots, m$, **return** $\mathbf{l}^{(k)}$ and $V^{(k)}$ as $\mathbf{l}$ and $\mathbf{V}$.

step s4 : **let** $\mathbf{l}^{(k+1)} = \mathbf{l}_p^{(k)}$ where $V_p^{(k)} \leq V_j^{(k)}$ for all $j = 1, \ldots, m$.

step s5 : **let** $k := k + 1$ and **goto step s1**.

procedure *FindSensorWithFixedLight*($\mathbf{v}, \mathbf{l}, \mathbf{V}$)

step l0 : **choose** the initial sensor position $\mathbf{v}^{(0)}$ and **let** $k := 0$.

step l1 : **find** the neighbors of $\mathbf{v}^{(k)}$ and **let** the neighbors be $\mathrm{N} = \{\mathbf{v}_1^{(k)}, \ldots, \mathbf{v}_m^{(k)}\}$.

step l2 : **for each** $\mathbf{v} \in \{\mathbf{v}^{(k)}\} \bigcup \mathrm{N}$, **call** *VarianceEvaluate*($\mathbf{v}, \mathbf{l}, \mathbf{V}$). **Let** the expected variances be called $V^{(k)}, V_1^{(k)}, \ldots, V_m^{(k)}$.

step l3 : **if** $V^{(k)} < V_j^{(k)}$ for all $j = 1, \ldots, m$, **return** $\mathbf{v}^{(k)}$ and $V^{(k)}$ as $\mathbf{v}$ and $\mathbf{V}$.

step l4 : **let** $\mathbf{v}^{(k+1)} = \mathbf{v}_p^{(k)}$ where $V_p^{(k)} \leq V_j^{(k)}$ for all $j = 1, \ldots, m$.

step l5 : **let** $k := k + 1$ and **goto step l1**.

procedure *VarianceEvaluate*($\mathbf{v}, \mathbf{l}, \mathbf{V}$)

step v1 : **for each** $e \in \mathrm{REL}_i$,

1. **for each** edge point $e_j \in e$,
   (a) **evaluate** C_j (contrast accross e_j) using equation 10,
   (b) **compute** σ_j^2 using equation 7.
2. **compute** $W = \sum 1/\sigma_j^2$, and $\mu_x, \mu_y, \sigma_x^2 + \sigma_y^2$,
3. **compute** variances of line parameters using equation 3.

step v2 : **compute** variances of intersection points using equation 5,

step v3 : **compute** variance of measurement $\mathrm{Var}(\mathbf{v}, \mathbf{l})$ using equation 6,

step v4 : **return** $\mathrm{Var}(\mathbf{v}, \mathbf{l})$ as $\mathbf{V}$.

FIGURE 8

alternating until the solution is found. They observed that this procedure converges to partial optimum solutions. In general, it does not converge to a local extremum; however, it can converge to a local extremum in many practical problems. Experimental results provided in [1, 6, 15, 17] demonstrate the efficiency of such an approach. We employ Wendell and Hurter's alternating approach to find our optimal sensor and light source position.

For each $\mathrm{REL}_i \in \mathrm{REL}$, we find the light source position $\mathbf{l}_i^{(1)}$ whose corresponding variance is minimum for a fixed sensor position $\mathbf{v}_i^{(0)}$. Next, we find the sensor position $\mathbf{v}_i^{(1)}$ whose corresponding variance is minimum for the light source position $\mathbf{l}_i^{(1)}$. We repeat this procedure by alternating the role of sensor position $\mathbf{v}$ and light source position $\mathbf{l}$ until the global minimum is found.

Once the optimal sensor and light source positions, $\mathbf{v}_i$ and $\mathbf{l}_i$ for each $\mathrm{REL}_i \in \mathrm{REL}$, are found, we choose the pair that has the minimum variance as the solution. In other words, the optimal sensor position $\mathcal{V}$ and light source position $\mathcal{L}$ satisfy the condition

$$\mathrm{Var}(\mathcal{V}, \mathcal{L}) \leq \mathrm{Var}(\mathbf{v}_i, \mathbf{l}_i) \quad \text{for all } i,$$

where $\mathrm{Var}(\mathbf{v}, \mathbf{l})$ denotes the variance of the measurement when the sensor is at $\mathbf{v}$ and the light source is at $\mathbf{l}$. The solution $(\mathcal{V}, \mathcal{L})$ satisfies the minimum variance criterion as well as the visibility requirement.

9. EXPERIMENTS AND RESULTS

The purpose of these experiments is to demonstrate that our approach to sensor and light source positioning is feasible and acceptable for practical use. The experiments consist of two parts.

1. ICE finds the optimal sensor and light source positions for the given measurements task. The sensor and light source positions that ICE found are denoted by $\mathcal{V}$ and $\mathcal{L}$, respectively.

2. We place the sensor and light source in various nonoptimal positions and take multiple pictures for each setting. We also put the sensor and light source at the optimal positions, sensor at $\mathcal{V}$ and light source at $\mathcal{L}$, and take multiple pictures. From these pictures, the variance of the measurement for each setting is estimated. Finally we check to see if the positions that ICE found are optimal (according to our criteria) by comparing the estimated variances of the measurements from the various nonoptimal settings to the variance from the optimal setting.

9.1. *Part I: ICE*

In **Task1** the given object is a 1.25 × 0.75 × 0.25 cm block and three of its sides are aligned along the three axes of the object coordinate system as shown in Fig. 6. The required measurement is the distance between the vertices v_3 and v_6.

Object Model. The surface equations for S_1, S_2, and S_3 are

$$f_1(x, y, z) = z - 0.25 = 0, \quad \text{where } 0 \le x \le 1.25,\ 0 \le y \le 0.75$$

$$f_2(x, y, z) = x - 1.25 = 0, \quad \text{where } 0 \le y \le 0.75,\ 0 \le z \le 0.25$$

$$f_3(x, y, z) = y - 0.75 = 0, \quad \text{where } 0 \le x \le 1.25,\ 0 \le z \le 0.25$$

The constants for its photometric properties are as follows: the fraction of specular reflectance $s = 0.1$ and the fraction of diffuse reflectance $d = 0.9$, diffuse constant $R_d = 1.0$, refractive index $n = 1.0$, extinction coefficient $k = 0.0$, surface roughness distribution follows Beckmann function with $m = 0.2$. These constants are from [3]. The light source chosen is an unpolarized point light source.

Required Edge List. Since we want to measure the distance between the vertices v_3 and v_6, the required edge list REL is given by Eq. (11). Namely,

$$\begin{aligned}\text{REL} = \{&\{e_2, e_4, e_6, e_7\}, \{e_2, e_4, e_6, e_{11}\}, \{e_2, e_4, e_7, e_{11}\},\\ &\{e_2, e_6, e_7, e_9\}, \{e_2, e_6, e_9, e_{11}\}, \{e_2, e_7, e_9, e_{11}\},\\ &\{e_4, e_6, e_7, e_9\}, \{e_4, e_6, e_9, e_{11}\}, \{e_4, e_7, e_9, e_{11}\}\},\end{aligned}$$

Contrast Evaluation. We chose 100 values of **r** varying y from 0.0 to 3.0 in steps of 0.03. Let the contrast at the ith point on the edge be C_i. Then the random perturbation of the ith edge point position is $k\sigma_\xi^2/C_i^2$. σ_ξ is unknown, and we chose a reasonable constant: $\sigma_\xi = 2.4$. Recall that the least-squares estimate of k is $\kappa^2 = 8.697$. Hence, the uncontrollable part of the random perturbation is $k\sigma_\xi \approx 50.0$. The contrasts for the other edges in each REL_i are computed similarly.

Variable Evaluation. Details of the variance evaluation procedure for a given edge list and sensor and light source positions were discussed in Section 8. There are nine elements in REL and for each element, we evaluate the variance in the same way. Let $\text{REL}_1 = \{e_4, e_7, e_9, e_{11}\}$. All the edges in REL_1 are straight lines. The variance of vertex position v_3, which is the intersection point of two edges e_4 and e_9, can now be computed using the variance of line parameters. The variance of the vertex position v_6, which is the intersection point of two edges e_7 and e_{11}, is computed similarly. Since we know the variance of two point positions, the variance of the distance between these two points can be computed via Eq. (6).

Optimization Procedure. Before attempting to find the optimal sensor and light source positions simultaneously, we examine the search space. First, the sensor position is fixed at (40°, 41°) in VS, and the variances of the distance between v_3 and v_6 for all possible light source positions in VS are computed.

We employ a drawing scheme for the search space in such a way that the center of the image is the gravitational center of a region of the search space where the variance is not infinite. The upper hemisphere of the reference sphere, whose north pole is at the chosen center, is projected down to its equator plane. Figure 9 shows the resulting representation of the search space. The straight lines represent the new longitudes, and the circles represent the new latitudes. The vertical line passing through the center of the picture also passes through the north pole of the reference sphere. Each pixel corresponds to a sensor or a light position in the viewing space VS. Its value represents the variance of the measurement. The lighter a pixel is, the smaller the variance is.

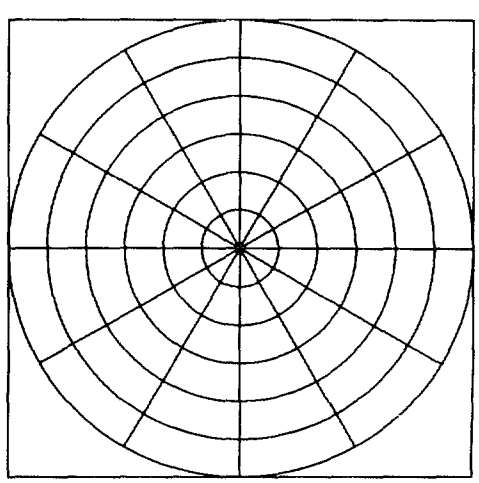

FIG. 9. The representation of the viewing space VS is illustrated.

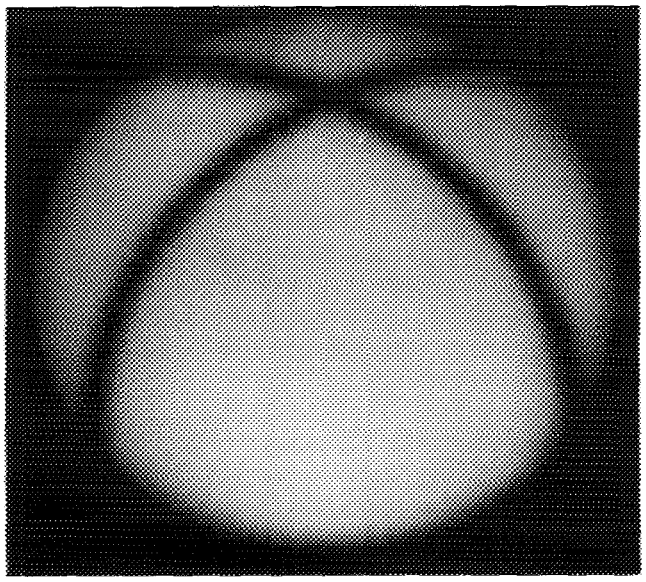

FIG. 10. The search space of **Task1**, which measures the distance between two vertices v_3 and v_6, is illustrated when the sensor is located at (40°, 41°) in VS. The center is (2°, 224°) in VS coordinates. Each pixel in the picture corresponds to a light position in the viewing space VS. Its value represents the variance of the measurement. The lighter a pixel is, the smaller the variance is. One can see the global minimum at around the center. Explicitly, the optimal light source position is (4°, 27°).

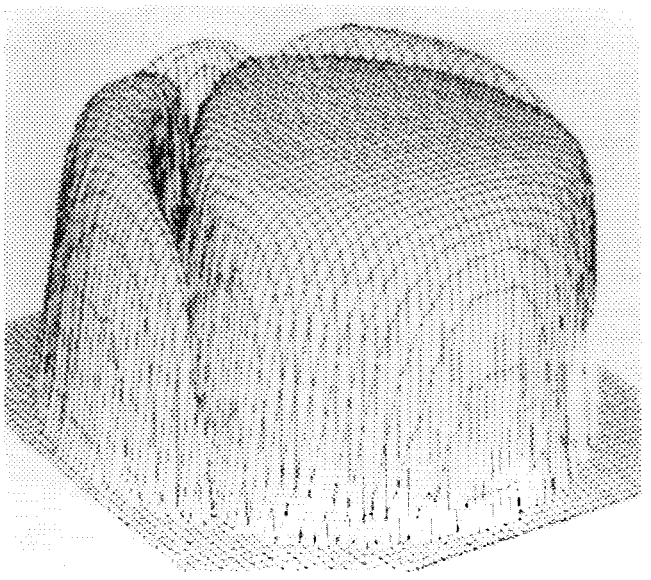

FIG. 11. A 3D plot of the picture which represents the search space of **Task1** when the sensor is located at (40°, 41°) in VS is illustrated. An inverted picture is used for this plot so that the maximum of this plot corresponds to the minimum of the original picture. It clearly shows that there is one and only one global minimum in the search space when the sensor is at the fixed location.

The optimal light source position is (11°, 52°) when the sensor is at (40°, 41°). Figures 10 and 11 illustrate the search space when the light source is fixed at (4°, 27°). Now the light source position is fixed at (4°, 27°) in VS, and ICE finds the optimal sensor position. Figures 12 and 13 illustrate the search space when the light source is fixed at (4°, 27°). As one can see, the search space is very flat, and there is little variation in the expected measurement variances. After two more iterations, ICE finds the optimal sensor and light source positions. Table 1 traces ICE's search.

9.2. *ICE vs Real*

Part II of the experiment consists of the comparison of the measurement variances from ICE and the analysis of error in the real images. The purpose of this experiment is to demonstrate that the optimal position that ICE found is really the optimal position. To do this, a total of 160 real pictures are taken. The variances of the measurements are estimated from the real pictures and compared with the variances that ICE found.

TABLE 1

Iteration	Fixed	Found	Variance
1	Sensor at (40°, 41°)	Light at (4°, 27°)	0.1023
2	Light at (4°, 27°)	Sensor at (32°, 140°)	0.0960
3	Sensor at (32°, 140°)	Light at (14°, 303°)	0.0703
4	Light at (14°, 303°)	Sensor at (32°, 140°)	0.0703

Note. ICE's Search Sequence for **Task1** is Traced When the Required Edge List is $REL_1 = \{e_4, e_9, e_7, e_{11}\}$.

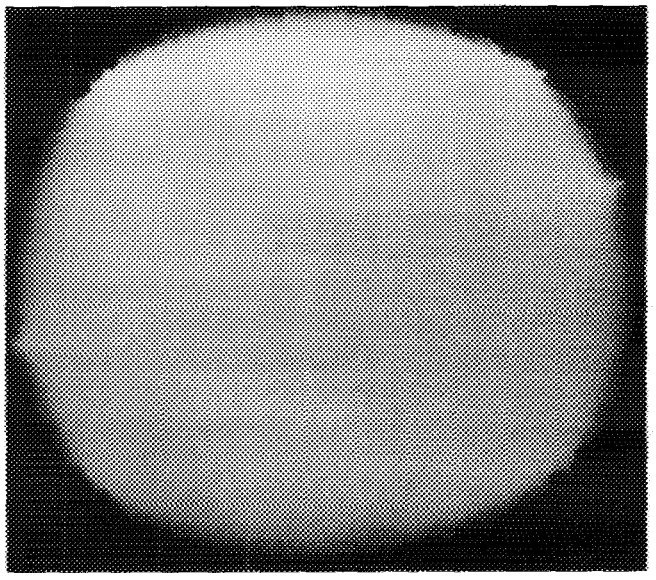

FIG. 12. The search space of **Task1**, which measures the distance between two vertices v_3 and v_6, is illustrated when the light source is located at (4°, 27°) in VS. The center is (0°, 49°) in VS coordinates. Each pixel in the picture corresponds to a sensor in the viewing space VS. Its value represents the variance of the measurement. The lighter a pixel is, the smaller the variance is. The optimal sensor position is (32°, 140°).

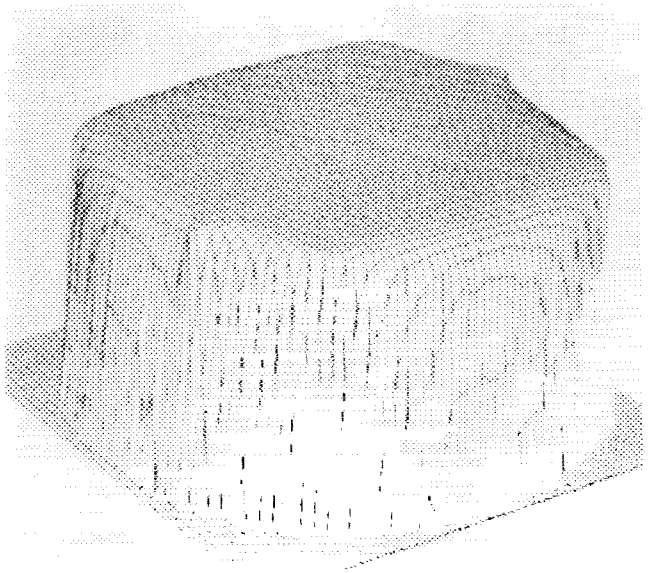

FIG. 13. A 3D plot of the picture which represents the search space of **Task1** when the light source is located at (4°, 27°) in VS is illustrated. An inverted picture is used for this plot so that the maximum of this plot corresponds to the minimum of the original picture.

TABLE 2

Sensor		Light source	
Polar angle	Azimuth angle	Polar angle	Azimuth angle
30°	90°	15°	270°
		60°	210°
		45°	270°
		30°	330°
30°	135°	15°	315°
		60°	255°
		45°	315°
		30°	15°
45°	225°	15°	45°
		30°	345°
		60°	45°
		45°	105°
60°	315°	60°	75°
		30°	135°
		45°	195°

Note. The chosen positions of sensor and light source for taking real images are shown.

Experimental Protocol. The reference sphere is assumed to have a radius of 100 cm. Since ICE assumes that the object lies along the reference frame and one of its vertices is at the origin of the reference frame, the northern hemisphere is sufficient for the viewing space. The setting is done in a dark room whose floor is carpeted in black. The floor is assumed to be the xy plane of the reference frame, and the object is placed on the floor. The object used in this experiment is a 12.5 × 7.5 × 2.5-cm sponge block. This sponge has more diffuse reflection than specular reflection, and the reflectance coefficients approximately match the parameters used for **Task1** in Part I.

Four sensor positions, including the optimal position, are chosen in the viewing space. For each sensor position, four light source positions, including the optimal position, are selected. The chosen positions are shown in Table 2. To place the sensor and light source in the designated place, we use plastic rulers to locate the correct position.

For each combination of four sensor and four light source positions, five pictures are taken on a Machine Vision International Genesis 2000 vision system. The point light source is simulated by mounting a 250-watt tungsten halogen projector lamp on a Pro-light P1-10, manufactured by Lowel-Light Manufacturing Inc., whose reflectors are coated in black. For the sensor, we use a CCD camera whose spatial resolution is 384 × 491 and gray scale is 0 to 255. The Genesis 2000 automatically changes the spatial image resolution to 480 × 512. The spatial resolution of each picture is reduced to 240 × 256 by chopping off the background.

The best one of five images of the objects involved in **Task1** for each sensor and light source setting is chosen for illustration. Figures 14, 16, 18, and 20 show the images of the object involved in **Task1** which are obtained

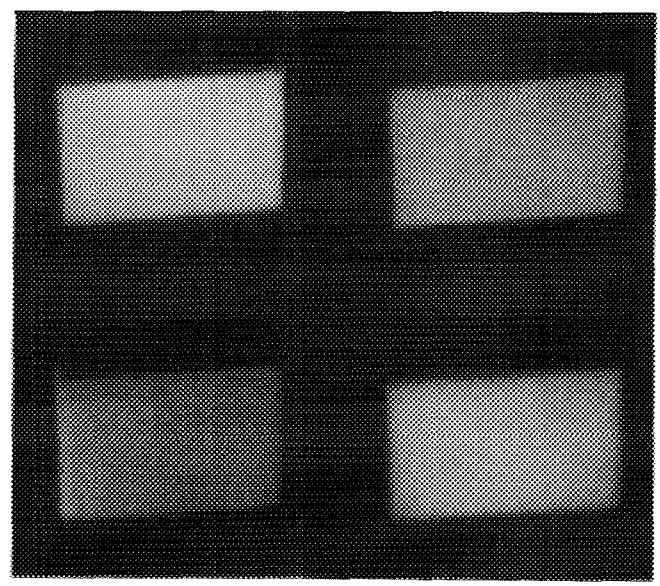

FIG. 14. The four real images of the 12.5 × 7.5 × 2.5-cm sponge block when the sensor is at (30°, 90°) is shown. The light source position of each image is as follows: top left (15°, 270°), top right (60°, 210°), bottom left (45°, 270°), bottom right (30°, 330°).

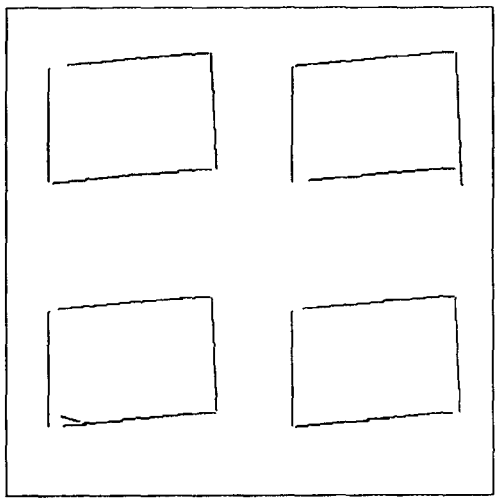

FIG. 15. The four edge images of the 12.5 × 7.5 × 2.5-cm sponge block when the sensor is at (30°, 90°) is shown. The light source position of each image is as follows: top left (15°, 270°), top right (60°, 210°), bottom left (45°, 270°), bottom right (30°, 330°).

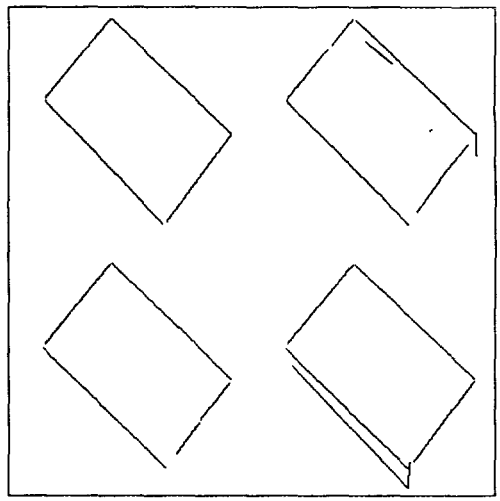

FIG. 17. The four edge images of the 12.5 × 7.5 × 2.5-cm sponge block when the sensor is at (30°, 135°) is shown. The light source position of each image is as follows: top left (15°, 315°), top right (60°, 255°), bottom left (45°, 315°), bottom right (30°, 15°).

when the sensor and light source are placed in the chosen positions. Figures 15, 17, 19, and 21 show edges extracted from each of those real images using GIPSY routines. The processings of each image produced four pairs of (θ, ρ), each representing one of the four side lines of the top rectangle of the given object, where θ is the rotational angle with respect to the column, and ρ is the Euclidean distance from the image origin, which is at the lower left corner. We compute the intersection points of each two of the four lines, and the distance between the two intersection points. For each sensor and light source setting, we had five real images and, therefore, five computed distance values. Since we did not know the true distance between the two intersection points, or vertices, the sample mean is used as the estimate of the true distance. Using this sample mean, the sample variance is

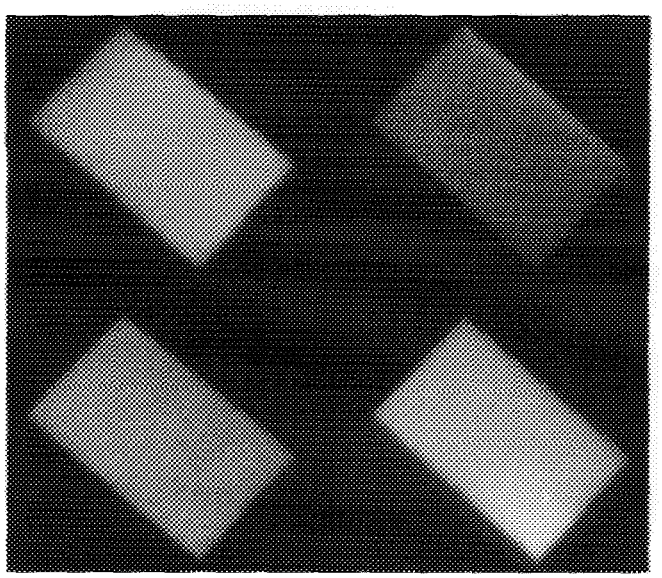

FIG. 16. The four edge images of the 12.5 × 7.5 × 2.5-cm sponge block when the sensor is at (30°, 135°) is shown. The light source position of each image is as follows: top left (15°, 315°), top right (60°, 255°), bottom left (45°, 315°), bottom right (30°, 15°).

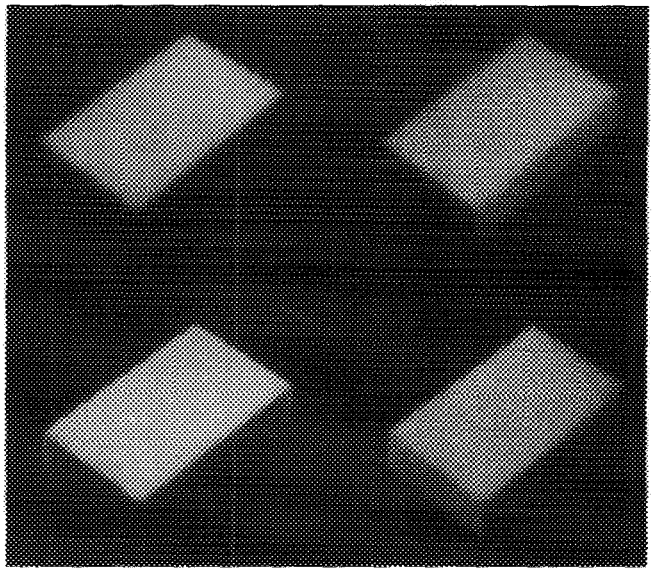

FIG. 18. The four real images of the 12.5 × 7.5 × 2.5-cm sponge block when the sensor is at (45°, 225°) is shown. The light source position of each image is as follows: top left (15°, 45°), top right (30°, 345°), bottom left (60°, 45°), bottom right (45°, 105°).

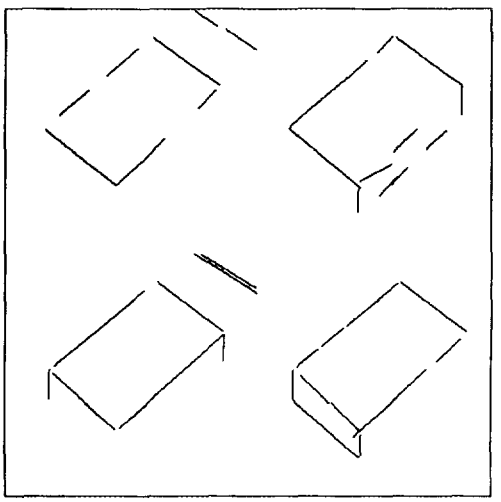

FIG. 19. The four edge images of the 12.5 × 7.5 × 2.5-cm sponge block when the sensor is at (45°, 225°) is shown. The light source position of each image is as follows: top left (15°, 45°), top right (30°, 345°), bottom left (60°, 45°), bottom right (45°, 105°).

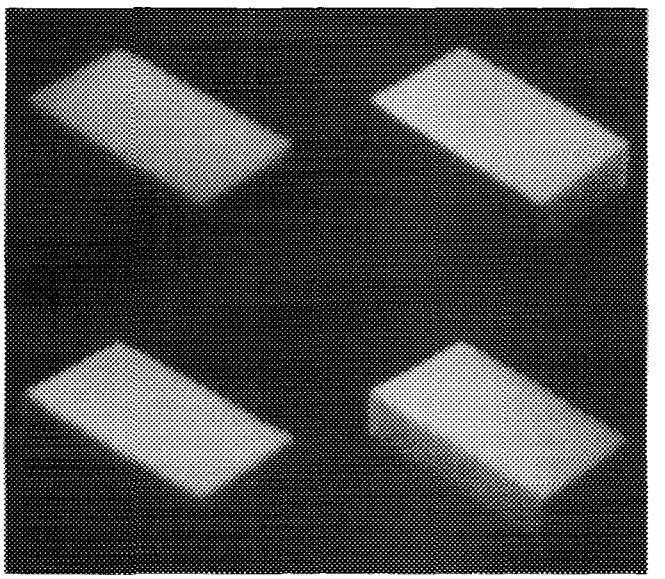

FIG. 20. The four real images of the 12.5 × 7.5 × 2.5-cm sponge block when the sensor is at (60°, 315°) is shown. The light source position of each image is as follows: top left (15°, 135°), top right (60°, 75°), bottom left (30°, 135°), bottom right (45°, 195°).

computed and is illustrated in Table 3. Two different threshold values, 12.0 and 10.0, were used in edge detection to see if the threshold affects the variance.

Although there are some discrepancies due to the small sample size, the two values, the variance from ICE and the variance computed from the real images, correlate. Due to the unknown noise, edge lines are either broken or totally lost in most settings when the sensor is placed at (45°, 225°) or at (60°, 315°). Since the parameters of the image processing operations were fixed, and also our sample size was not large enough, we did not succeed in estimating the variance for those settings precisely. However, the correlation coefficient between the variance that ICE produced and the variance that was computed from the real images is 0.768, which means they correlate reasonably well. Most importantly, the variance from the

TABLE 3

Sensor at	Light at	Variance from ICE	Variance from real pictures threshold = 12.0	Variance from real pictures threshold = 10.0
(30°, 90°)	(15°, 270°)	0.079	0.386	0.386
(30°, 90°)	(60°, 210°)	0.352	0.101	0.101
(30°, 90°)	(45°, 270°)	0.157	0.096	0.096
(30°, 90°)	(30°, 330°)	0.094	0.091	0.085
(30°, 135°)	(15°, 315°)	0.070	0.010	0.010
(30°, 135°)	(60°, 255°)	0.595	0.348	0.324
(30°, 135°)	(45°, 315°)	0.133	0.190	0.196
(30°, 135°)	(30°, 15°)	0.084	0.969	1.911
(45°, 225°)	(15°, 45°)	0.120	0.717	1.557
(45°, 225°)	(30°, 345°)	0.164	N/A	N/A
(45°, 225°)	(60°, 45°)	0.423	N/A	N/A
(45°, 225°)	(45°, 105°)	0.283	N/A	N/A
(60°, 315°)	(15°, 135°)	0.099	N/A	N/A
(60°, 315°)	(60°, 75°)	0.323	4.352	4.973
(60°, 315°)	(30°, 135°)	0.189	N/A	N/A
(60°, 315°)	(45°, 195°)	0.148	1.401	1.312

Note. Variances that ICE computes and variances from the real images are compared when the given task is **Task1.** * denotes the optimal position.

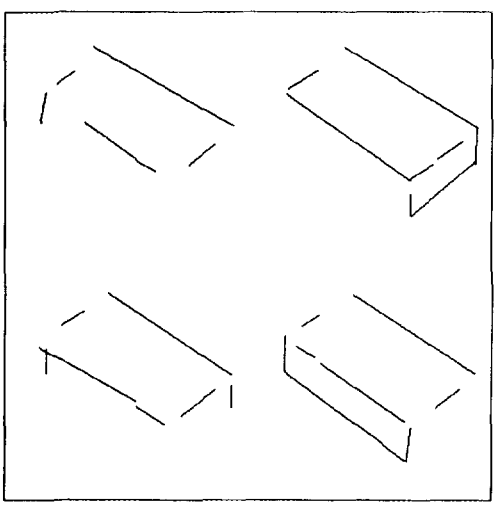

FIG. 21. The four edge images of the 12.5 × 7.5 × 2.5-cm sponge block when the sensor is at (60°, 315°) is shown. The light source position of each image is as follows: top left (15°, 135°), top right (60°, 75°), bottom left (30°, 135°), bottom right (45°, 195°).

real picture which was taken at the optimal position is minimal as ICE expected.

10. CONCLUSION

An optimization approach to automatic sensor and light source positioning for a machine vision task, where geometric measurement and/or object verification is important, was described. The goal of the vision task was specified in terms of measurements related to edges. The optimal sensor and light source positions were defined as the positions which produce an image from which we can obtain the measurement data with the minimum variance. To demonstrate that our optimization approach is feasible and acceptable for practical use, a software system called ICE has been designed and implemented. A series of experiments was conducted to show that the positions that ICE found are really the optimal positions.

The results show that the optimization problem we formulated is nearly a convex problem, and therefore it can be easily solved by mathematical programming techniques. The positions that ICE found are also the best positions found in the real experiments. Furthermore, the correlation coefficient between the variance that ICE expected and the variance computed from the real images was 0.768.

There are several directions in which ICE can be extended. When the goal of the vision task cannot be satisfied with a single sensor, multiple sensors may be employed. Also if the goal of the vision task cannot be met with a single light source, multiple light sources may be employed. In both cases, the interaction effect of multiple sensors and multiple light sources must be carefully analyzed. The reflectance coefficient can be modeled in such a way that it is not uniform but is of functional form. The analysis of error propagation for the case of lines, circles, and ellipses has been done, and it can be extended further to other general quadratic curves and to cover noise distributions other than Gaussian noise. This optimization problem may also be extended to include other important factors like polarization of light source, polarization of sensor, and wavelength band of light source.

REFERENCES

1. Y. Bar-Shalom, Optimal simultaneous state estimation and parameter identification in linear discrete-time systems, *IEEE Trans. Autom. Control* **17**, 1972, 308–319.
2. B. G. Batchelor, *A Prolog Lighting Advisor*, School of Electrical, Electronic, and Systems Engineering, University of Wales College of Cardiff, 1989.
3. R. L. Cook, and K. E. Torrance, A reflectance model for computer graphics, *ACM Trans. Graphics* **1**(1), 7–24.
4. C. K. Cowan, and P. D. Kovesi, Automatic sensor placement from vision task requirements, *IEEE Trans. Pattern Anal. Mach. Intell.* **10**(3), 1988, 407–416.
5. I. Faux, and M. Pratt, *Computational Geometry for Design and Manufacture*, Wiley, New York, 1979.
6. J. Goutsias, and J. M. Mendel, Optimal simultaneous detection and estimation of filtered discrete semi-Markov chains, *IEEE Trans. Inf. Theory* **34**, 1988, 551–568.
7. R. M. Haralick, Digital step edges from zero crossing of second directional derivatives, *IEEE Trans. Pattern Anal. Mach. Intell.* **PAMI-6**(1) 1984, 58–68.
8. R. M. Haralick, Line fitting, Unpublished manuscript, Intelligent Systems Laboratory, Department of Electrical Engineering, University of Washington, Seattle, 1989.
9. R. M. Haralick and L. G. Shapiro, *Computer and Robot Vision: Volume II*, Addison–Wesley, Reading, MA, 1993.
10. R. M. Haralick and L. Watson, A facet model for image data, *Comput. Graphics Image Process.* **15** 1981, 113–129.
11. E. E. Hartquist and H. A. Marisa, *PADL-2 User's Manual*, The Production Automation Project, The University of Rochester, Rochester, NY, 1985.
12. K. Ikeuchi, Generating an interpretation tree from a cad model to represent object configurations for bin-picking tasks, Technical Report CMU-CS-86-144, Computer Science Department, Carnegie Mellon University, Pittsburgh, PA, July 1986.
13. K. Ikeuchi and T. Kanade, Modeling sensor detectability and reliability in the configuration space for model-based vision, Technical Report CMU-CS-87-144, Computer Science Department, Carnegie Mellon University, Pittsburgh, PA, July 1987.
14. K. Ikeuchi and T. Kanade, Applying sensor models to automatic generation of object recognition programs, in *Proceedings of the Second International Conference on Computer Vision, Tampa, FL, December 1988*, pp. 228–237.
15. J. Kormylo and Mendel, J. M. Maximum-likelihood detection and estimation of Bernoulli-Gaussian processes. *IEEE Transactions on Information Theory 28* (1982), 482–488.
16. E. Krotokov, Focusing, Technical Report MS-CIS-86-22, Department of Computer and Information Science, University of Pennsylvania, Philadelphia, PA, April 1986.
17. S. Lakshmann and H. Derin, Simultaneous parameter estimation segmentation of Gibbs random fields wing simulated annealing, *IEEE Trans. Pattern Anal. Mach. Intell.* **11**, 1989, 799–813.
18. W. Newman and R. Sproull, *Principles of Interactive Computer Graphics*, McGraw–Hill, Tokyo, 1981.
19. R. Niepold and S. Sakane, VIO—An approach to vision sensor and illumination planning using environmental models. Submitted to Computer Vision, Graphics and Image Processing, 1988.
20. A. Novini, Penn Video Lighting Advisor, 1988.
21. A. P. Pentland, A new sense for depth of field, in *Proceedings of the Ninth International Joint Conference on Artificial Intelligence, Los Angeles, CA, August 1985*, pp. 988–994.
22. A. Rosenfeld and A. C. Kak, *Digital Picture Processing*, Academic Press, New York, 1982.
23. Y. Shirai and S. Tsuji, Extraction of the line drawing of 3-dimensional objects by sequential illumination from several directions, *Pattern Recognit.* **4**, 1972, 343–351.
24. R. E. Wendell and A. P. Hurter, Minimization of a non-separable objective function subject to disjoint constraints, *Oper. Res.* **24**(4) 1976, 643–657.
25. S. Yi, Illumination Control Expert for Machine Vision: A Goal

Driven Approach, Ph.D. Dissertation, Department of Computer Science and Engineering, University of Washington, Seattle, WA, March 1990.

26. S. Yi, R. M. Haralick, and L. G. Shapiro, An illumination model for machine vision, Technical Report EE-ISL-89-02, Intelligence Systems Laboratory, Department of Computer Science and Engineering, University of Washington, Seattle, WA, September 1989.
27. S. Yi, R. M. Haralick, and L. G. Shapiro, Automatic sensor and light source positioning for machine vision, in *Proceedings of the 10th International Conference on Pattern Recognition, Atlantic City, NJ, June 1990.*
28. S. Yi, R. M. Haralick, and L. G. Shapiro, Error propagation in machine vision, in *Machine Vision and Applications, 7* (1994), 93–114.